General Disclaimer

One or more of the Following Statements may affect this Document

- This document has been reproduced from the best copy furnished by the organizational source. It is being released in the interest of making available as much information as possible.

- This document may contain data, which exceeds the sheet parameters. It was furnished in this condition by the organizational source and is the best copy available.

- This document may contain tone-on-tone or color graphs, charts and/or pictures, which have been reproduced in black and white.

- This document is paginated as submitted by the original source.

- Portions of this document are not fully legible due to the historical nature of some of the material. However, it is the best reproduction available from the original submission.

NASA TECHNICAL MEMORANDUM

NASA TM X-72785

NASA TM X-72785

(NASA-TM-X-72785) SOME RECENT APPLICATIONS OF THE SUCTION ANALOGY TO VORTEX-LIFT ESTIMATES (NASA) 37 p HC $4.00 CSCL 01A

N76-18040

Unclas
G3/01 18451

SOME RECENT APPLICATIONS OF THE SUCTION ANALOGY TO VORTEX-LIFT ESTIMATES

By

John E. Lamar

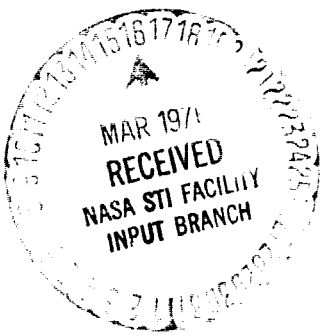

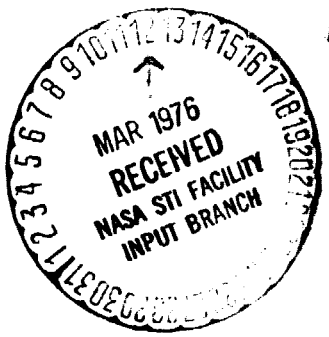

NATIONAL AERONAUTICS AND SPACE ADMINISTRATION
LANGLEY RESEARCH CENTER, HAMPTON, VIRGINIA 23665

1. Report No.	2. Government Accession No.	3. Recipient's Catalog No.
TM X-72785		

4. Title and Subtitle	5. Report Date
SOME RECENT APPLICATIONS OF THE SUCTION ANALOGY TO VORTEX-LIFT ESTIMATES	February 1976
	6. Performing Organization Code
7. Author(s)	8. Performing Organization Report No.
John E. Lamar	10. Work Unit No.
9. Performing Organization Name and Address	11. Contract or Grant No.
NASA Langley Research Center Hampton, VA 23665	13. Type of Report and Period Covered
12. Sponsoring Agency Name and Address	14. Sponsoring Agency Code
National Aeronautics and Space Administration Washington, DC 20546	

15. Supplementary Notes

This paper originally appeared in Aerodynamic Analyses Requiring Advanced Computers, Part II, NASA SP-347, pages 985 - 1011, March 4-6, 1975.

16. Abstract

This paper reviews a recent extension of the suction analogy for the estimation of vortex lift along the side edge of wings and develops the concept of an augmented vortex lift to account for the effect of the leading-edge vortex passing downstream over an aft part of the model. Applications of these extensions have resulted in an improved estimating capability for a wide range of isolated sharp-edge planforms and also for multiple lifting surfaces. Hence, the suction analogy concept can now have wider applicability at both subsonic and supersonic speeds, especially in the preliminary design cycle.

17. Key Words (Suggested by Author(s)) (STAR category underlined)	18. Distribution Statement
vortex lift suction analogy subsonic supersonic generalized planforms	Unclassified - Unlimited STAR Category 01

19. Security Classif. (of this report)	20. Security Classif. (of this page)	21. No. of Pages	22. Price*
Unclassified	Unclassified	27	$3.75

*Available from { The National Technical Information Service, Springfield, Virginia 22151
STIF/NASA Scientific and Technical Information Facility, P.O. Box 33, College Park, MD 20740

SOME RECENT APPLICATIONS OF THE SUCTION ANALOGY TO VORTEX-LIFT ESTIMATES

By John E. Lamar
NASA Langley Research Center

SUMMARY

This paper reviews a recent extension of the suction analogy for the estimation of vortex lift along the side edge of wings and develops the concept of an augmented vortex lift to account for the effect of the leading-edge vortex passing downstream over an aft part of the model. Applications of these extensions have resulted in an improved estimating capability for a wide range of isolated sharp-edge planforms and also for multiple lifting surfaces. Hence, the suction analogy concept can now have wider applicability at both subsonic and supersonic speeds, especially in the preliminary design cycle.

INTRODUCTION

In the design and analysis of high-speed aircraft, a detailed knowledge of the effects of flow separation is required, particularly with regard to critical wing loads and the stability and performance at various off-design conditions. Since attached-flow theories are inadequate for these conditions, the designer currently must rely on extensive and costly wind-tunnel tests which include detailed pressure distributions. In many cases, wind-tunnel tests occur too late in the cycle to impact the important aero/structural design trade-offs. One class of separation which is often encountered is leading- and side-edge separation and the resulting vortex-lift phenomena which are important with regard to the aero/structural trade-offs and also are being increasingly utilized to improve the maneuvering capability of fighters.

In reference 1, Polhamus introduced the concept of a suction analogy for estimation of the lift which arises from separated flow around sharp-edge delta wings reattaching on the upper surface (called vortex flows). The suction analogy states that the potential-flow leading-edge suction force, which no longer acts in the chord plane when leading-edge separation exists, is reoriented on the upper surface (rotated 90^{o}) by the vortex flow action and thereby provides an additional normal force. Because of the change in direction of the suction force, the normal force is now the resultant aerodynamic force.

Figure 1 shows an example of a 75^{o} swept sharp-edge delta wing at a low subsonic Mach number taken from reference 2. The plot of lift as a function of angle of attack

shows the large vortex lift which is well estimated by the suction analogy method. Also shown is the variation of vortex drag with lift and the data are again well estimated by the theory.

After the original application of the suction analogy to delta wings, it was applied to other pointed wings at subsonic speeds (refs. 3 and 4) and to delta wings at supersonic speeds (ref. 4).

This paper deals with recent applications of the suction analogy to more generalized configurations as shown in figure 2. As in the earlier application, the configurations are limited to planforms with sharp edges. At subsonic speeds, applying the analogy to the side edges of planforms leads to an estimate of the vortex lift associated with side-edge vortex flows. Analysis of this estimate has led to the concept of an augmented vortex lift. At supersonic speeds the effects of Mach number and high angle of attack are discussed for delta wings, evidence of vortex lift along the side edge of a rectangular wing is presented, and its magnitude determined. The vortex lift arising on multiple lifting surfaces, such as complete aircraft configurations, can also be treated by the suction analogy.

Subsonic solutions can be computed for potential-flow problems having matrix sizes less than 200×200 with the CDC digital computer in about three minutes and require a core of 53000_8. Supersonic solutions obtained with the supersonic linearized theory can be written in closed form.

SYMBOLS

A	aspect ratio
b	wing span
C_D	drag coefficient, $\frac{\text{Drag}}{q_\infty S_{ref}}$
$C_{D,o}$	experimental value of drag coefficient at $C_L = 0$
C_L	lift coefficient, $\frac{\text{Lift}}{q_\infty S_{ref}}$
ΔC_L	C_L increment associated with augmented vortex lift

C_m pitching-moment coefficient about reference point which is located at $\frac{c_{ref}}{4}$ unless otherwise stated, $\frac{\text{Pitching moment}}{q_\infty S_{ref} c_{ref}}$

C_N normal-force coefficient, $\frac{\text{Normal force}}{q_\infty S_{ref}}$

$\Delta C_{p,u}$ change in upper surface pressure coefficient from its value at $\alpha = 0^o$, $\frac{\text{Change in upper surface pressure}}{q_\infty}$

C_S leading-edge suction-force coefficient, $K_{v,le} \sin^2 \alpha$

c streamwise chord

$\tilde{c}$ characteristic length used in determination of $\bar{K}_{v,se}$

c_n section normal-force coefficient, $\frac{\text{Section normal force}}{q_\infty c}$

c_s section suction-force coefficient, $\frac{\text{Section suction force}}{q_\infty c}$

dF_S differential leading-edge suction force (fig. 5)

$f_{s,se}$ distributed side-edge suction force

$f'_{s,se}$ $= \frac{2f_{s,se}(\Delta x')}{bq_\infty \alpha^2}$

K_p potential-lift factor, $\frac{\partial (C_{N,p})}{\partial (\sin \alpha \cos \alpha)}$

$K_{v,le}$ leading-edge-vortex-lift factor,

$$\frac{\partial \left(\frac{2 \text{ Leading-edge suction force from one edge}}{q_\infty S_{ref}} \right)}{\partial \sin^2 \alpha}$$

$K_{v,se}$ side-edge-vortex-lift factor, $\dfrac{\partial\left(\dfrac{\text{2 Side-edge suction force from one edge}}{q_\infty S_{ref}}\right)}{\partial \sin^2 \alpha}$

$\overline{K}_{v,s\epsilon}$ augmented-vortex-lift factor, $\dfrac{K_{v,le}}{(b/2)\sec \Lambda}\tilde{c}$

l distance along leading edge from apex

M free-stream Mach number

q_∞ free-stream dynamic pressure

S surface area

U free-stream velocity

u induced velocity in x-direction at point (x,y)

v induced velocity in y-direction at point (x,y)

w_{net} sum of induced downwash and $U\alpha$ at $\alpha = 1$ rad

$\overline{w}_{net}$ average value of w_{net}

x,y,z distances from a coordinate origin located at leading-edge apex; x positive downstream, y positive toward right wing tip, z positive up

x/c fractional distance along streamwise chord

Δx distance along tip chord

$\Delta x'$ $= \Delta x/c_t$

α angle of attack

α_D departure angle of attack

Γ equivalent circulation associated with leading-edge suction

$\overline{\Gamma}$ average value of Γ

γ distributed bound vorticity at point (x,y)

δ distributed trailing vorticity at point (x,y)

δ_t tip rake angle, positive as trailing-edge tip moves inboard

ρ density of fluid

Λ leading-edge sweep angle, positive for sweepback

λ taper ratio, $\frac{c_t}{c_r}$

μ $= \sin^{-1}\left(\frac{1}{M}\right)$

ϕ dihedral angle, positive for wing tip up

Subscripts:

av average

c centroid

i particular item of location

*l*e leading edge

p potential or attached flow

r root

ref reference; for S, true wing area; for c, mean geometric chord

se side edge

t	tip
tot	total
vle	vortex effect at leading edge
vse	vortex effect at side edge
w	wing

SIDE-EDGE VORTEX LIFT

Concept

The suction analogy is not limited to vortex flows around the leading edge but can be applied wherever singularities in the potential-flow induced velocities produce an edge force. Figure 3 shows that this can occur along the side edges because of the singularities in v. Hence, with vortex flows associated with separation around the side edges, the forces no longer act in the wing plane but in the normal-force direction as in leading-edge separation.

A mathematical procedure for computing this side force has been developed for wings at subsonic speeds, initially, and is given in reference 5. The procedure employs the modified Multhopp method of reference 6 to provide the information needed to begin the side-force computation. In addition, three discrete-loading analyses employing the vortex-lattice method (refs. 7, 8, and 9) have been made and are discussed in reference 9. In reference 9, the vortex-lattice method is shown to yield results in close agreement with those of reference 5; hence, the reference 9 method is utilized in this report for some isolated planforms and all subsonic configurations for which the reference 5 method is not appropriate. Initially, the effect of the side-edge vortex lift is combined with the leading-edge and the potential-flow effects to yield estimates which are denoted on some figures as those of the present method. (Subsequently, the present method includes the augmented vortex lift as well.)

The following equations relate the potential- and vortex-lift factors to C_L, C_D, and C_m:

$$C_L = \overbrace{K_p \sin\alpha \cos^2\alpha}^{C_{L,p}} + \overbrace{K_{v,le} \sin^2\alpha \cos\alpha}^{C_{L,vle}} + \overbrace{K_{v,se} \sin^2\alpha \cos\alpha}^{C_{L,vse}} \quad (1)$$

or

$$C_L = K_p \sin \alpha \cos^2 \alpha + K_{v,tot} \sin^2 \alpha \cos \alpha \tag{2}$$

$$C_D = C_{D,o} + C_L \tan \alpha = C_{D,o} + K_p \sin^2 \alpha \cos \alpha + K_{v,tot} \sin^3 \alpha \tag{3}$$

and

$$C_m = \overbrace{K_p \sin \alpha \cos \alpha \frac{\bar{x}_p}{c_{ref}}}^{C_{m,p}} + \overbrace{K_{v,le} \sin^2 \alpha \frac{\bar{x}_{le}}{c_{ref}}}^{C_{m,vle}} + \overbrace{K_{v,se} \sin^2 \alpha \frac{\bar{x}_{se}}{c_{ref}}}^{C_{m,vse}} \tag{4}$$

where the particular $\bar{x}$-terms equal $x_{ref} - x_{c,i}$ for i equal to p, *le*, and se. In this paper, x_{ref} is the quarter-chord location of the mean geometric chord.

Application

Figure 4 presents a comparison of experimental and theoretical subsonic aerodynamic characteristics of an $A = 1$ rectangular wing. Also shown are the potential- and vortex-lift factors and lift increments determined in reference 5. The figure shows that the present method estimates the C_L experimental data of reference 5 better than the other methods. (See ref. 5 for a discussion of the methods in refs. 10, 11, 12, and 13.) This figure also shows that the $C_{m,le}$ experimental data are better estimated by the present method up to $\alpha \approx 16^o$. For higher angles of attack, the data show a larger nose down moment than the present estimate. This comparison indicates the magnitude of the error introduced by the present method in assuming that the potential and vortex lifts, in particular the leading-edge one, do not move with increasing α.

With the vortex lift from the side edge identified, its magnitude estimated, and good agreement with experimental data shown, the vortex lifts on more generalized planforms are now studied.

AUGMENTED VORTEX LIFT

Concept

The concept of augmented vortex lift arises from the well-established fact that for many delta wings the leading-edge vortex generated on the wing persists for a considerable distance downstream and therefore can act on other surfaces, such as the aft part of more generalized planforms or aircraft horizontal tails. This persistence is not accounted for in the suction analogy because the analogy deals only with the edge forces generated along a particular edge, such as leading-edge vortex lift resulting from the leading-edge suction force. Figure 5 shows examples of two systems employed that

account for vortex lift on delta and cropped-delta wings. They are (1) a theoretical one developed from a planar potential theory and utilizing the suction analogy and (2) a more realistic (actual) one that is due to action of the leading-edge shed vortex. The following important points are made from this figure: (1) the leading-edge suction distribution has a peak value somewhere along the leading edge away from the extremes and goes to zero at the tip because no edge forces are present beyond the point of maximum span; (2) for the cropped-delta wing, the aft part of the wing can generate additional (augmented) vortex lift because of the presence of the leading-edge vortex (as discussed in ref. 14); and (3) the side-edge suction distribution generally peaks near the trailing edge and is discussed subsequently.

Estimating Procedure

In order to estimate the augmented vortex lift, it is first necessary to quantify the circulation of the shed vortex along the wing leading edge. This can be done as indicated by the lower sketch on figure 5. The Kutta-Joukowski Law has been employed to relate the differential suction force along the leading edge to an unknown circulation $\Gamma(\ell)$. By a coordinate transformation, it can also be related to the leading-edge suction distribution along the span as

$$\frac{c_s c(y)}{\alpha^2} = -2 \sec \Lambda \frac{\Gamma w_{net,le}(y)}{\alpha^2 U^2} \tag{5}$$

Figure 6 shows an idealized distribution of the product $\frac{-\Gamma w_{net,le}}{\alpha^2 U^2}$ along with a fairly reasonable $\frac{-w_{net,le}}{U}$ (upwash) distribution for a cropped-delta wing. As a consequence, $\frac{\Gamma}{\alpha^2 U}$ can be estimated as shown. Because the actual circulation does not go to zero (hence the vortex persists downstream), the distribution of circulation cannot be used. Instead, an average value is employed. With an average value used for $\frac{\Gamma}{\alpha^2 U}$, it is consistent to utilize an average value for $\frac{-w_{net,le}}{U}$ as well. This result can be expressed in terms of the leading-edge-vortex-lift factor by

$$\int_0^{b/2} \frac{c_s c \, dy}{\alpha^2} = \frac{K_{v,le}}{2} S_{ref} = -2 \sec \Lambda \frac{\bar{\Gamma} \bar{w}_{net,le}}{\alpha^2 U^2} \frac{b}{2} \tag{6}$$

Hence,

$$\frac{\bar{\Gamma}}{\alpha^2 U} = \frac{-K_{v,le} S_{ref}}{2b \sec \Lambda \frac{\bar{w}_{net,le}}{U}} \tag{7}$$

Employing this result in the Kutta-Joukowski Law, this time along the side edge, permits the estimation of the augmented vortex lift. The details are

$$\frac{\text{Augmented vortex lift along one edge}}{\alpha^2} = -\rho \bar{w}_{net,se} \frac{\bar{\Gamma}}{\alpha^2} \tilde{c} \tag{8}$$

where the $\frac{-w_{net,se}}{U}$ distribution and its average are again reasonably depicted at the bottom right of figure 6 and $\tilde{c}$ is a characteristic streamwise length. By inspection of figure 6

$$\frac{\bar{w}_{net,se}}{U} \approx \frac{\bar{w}_{net,le}}{U} \tag{9}$$

Then defining the left side of equation (8) as $\frac{\bar{K}_{v,se}}{2} q_\infty S_{ref}$ leads to

$$\frac{\bar{K}_{v,se}}{2} q_\infty S_{ref} = q_\infty \frac{K_{v,le}}{b \sec \Lambda} S_{ref} \tilde{c} \tag{10}$$

or

$$\bar{K}_{v,se} = \left[\frac{K_{v,le}}{(b/2) \sec \Lambda} \right] \tilde{c} \tag{11}$$

The term in brackets results from the use of average values and amounts to assuming that the leading-edge-vortex-lift factor is developed at a constant rate along the leading-edge length $(b/2) \sec \Lambda$. For cropped-delta wings the value of $\tilde{c}$ is taken to be the length of the tip chord.

Applications

Cropped-delta wings.- Figure 7 presents an application of the augmented vortex lift to a cropped-delta wing of $\Lambda = 45^o$ and $\lambda = 0.5$. The value of $\bar{K}_{v,se}$ is about two-thirds of the other vortex-lift factors, and its inclusion leads to improved agreement with both the C_L and the C_m experimental data. (For C_m estimates the augmented vortex lift is applied at the centroid of the side-edge suction distribution for cropped-delta wings and at the centroid of additional area behind or ahead of the delta part for pointed wings.)

At this taper ratio ($\lambda = 0.5$), C_L is reasonably well predicted over the range of α from 0^o to 20^o. Above $\alpha = 20^o$ the data fall below the theory curve. The angle of attack at which this occurs is called the departure angle α_D herein, and it is graphed as a function of aspect ratio for this wing and other cropped-delta wings in this same series which have a leading-edge sweep of 45^o. The others have taper ratios of 0.4, 0.3, 0.2, 0.1, and 0. For comparison, the departure angles of sharp-edge delta wings are

also graphed (from ref. 2), and the addition of area behind the moderately swept delta ($\Lambda = 45^{o}$) increases the departure angle, just as increasing the sweep on a delta wing does. The explanation of the variation of α_D with A is hypothesized to be related to at least the leading-edge suction distribution and possibly to the side-edge suction distribution.

In order to determine the relationships, the cropped-delta leading-edge and side-edge suction distributions are presented in figures 8 and 9, respectively. For comparison, the leading-edge suction distributions for three delta wings are also presented in figure 8 (the upper two from ref. 15). For both sets the peak values of leading-edge suction distribution become larger and occur at a more outboard location with decreasing A. Hence, it can be stated that as the leading-edge suction distribution becomes more triangular, the angle of attack for departure increases.

Figure 9 shows that the side-edge suction distribution increases for increasing taper ratio and does not tend to zero at the trailing edge. The increase could be expressed in terms of an increase in circulation along the side edge by an analogous approach to that employed previously and would translate into a stronger "tip vortex." This increase could also be thought of as providing a favorable pressure gradient for the leading-edge vortex acting near the tip, so that a vortex flow would be produced there where an unorganized flow had existed previously. The reason that the side-edge suction does not go to zero at the trailing edge is that this suction force can be sustained along the edge of the trailing planar vortex sheet (ref. 16), unlike the spanwise extension of the leading-edge suction as discussed previously.

Generalized planforms.- Figures 10 and 11 present additional examples of the augmented-vortex-lift concept for wings with pointed and streamwise tips, respectively. (Some data of fig. 10 were taken from ref. 17.) The value of $\tilde{c}$ used in the computation of $\bar{K}_{v,se}$ was determined empirically to be the streamwise distance from the trailing edge of the root chord to the leading edge of the wing tip. (Positive $\tilde{c}$ values occur for wings such as the diamond type.) This definition of $\tilde{c}$ enables one definition to be used for all wings, including the cropped ones. It should be noted that of the eight examples shown in these two figures, $\tilde{c}$ is positive for all but two. The negative values can be thought of as due to the lack of complete flow reattachment on the more arrowlike wings.

From the examples presented, it can be seen that addition of the augmented vortex lift improves the agreement of the theory with the data at least slightly and more often significantly.

OTHER APPLICATIONS

Figure 12 shows two attempts to improve the vortex lift on pointed wings of low sweep by altering the planform along the leading edge. In each instance it was postulate

that by doing so the moderate-sweep leading-edge vortex system could be strengthened and thereby provide additional lift to higher values of α. The first attempt (top right) involved serrating the leading edges, but this resulted in two vortexes of opposite circulation being shed at each concave juncture. From the figure, it can be seen that this attempt was not successful.

The second attempt (bottom right) was to cause all of the shed vortexes along a leading edge to be shed in the same direction in order to eliminate the previous difficulty. However, comparison with the results for the basic delta wing (bottom left) shows that this attempt offered no significant improvement and hence can also be classified as unsuccessful.

Figure 13 presents the experimental and theoretical C_L values for a cropped-delta wing with varying tip rake angles δ_t. They are compared at two angles of attack and, in general, for each α the data fall between the two theory curves. The curve labeled "both side edges" is shown for reference and is simply the $\delta_t = 0$ result extended over the δ_t range. The other curve labeled "one side edge" is the asymmetrical wing solution[1] with only one side edge contributing to vortex lift. For each curve the contributions of potential lift and leading-edge, side-edge, and augmented vortex lift are summed. The conclusions from this figure are that: (1) the data are reasonably well estimated; and (2) rake angles $\delta_t \geq 13^\circ$ are necessary for the data to no longer exhibit an effective "side edge."

SUPERSONIC RESULTS

Delta Wings

The suction analogy has been applied to delta wings at supersonic speeds in reference 4; however, some more recent applications, such as the ones in reference 19, raise points which require attention. Figure 14 from reference 20 helps to illustrate the points. Like the $A = 1$ sharp-edge delta wing of reference 4, the $A = 1.1$ sharp-edge delta wing in this figure shows a similar reduction in the vortex lift available with increasing M. This is because the upwash field between the Mach cone and the wing leading edge becomes more restricted with the increase in M, thereby leading to a reduction in $K_{v,le}$. In addition, the angle of attack for departure decreases with increasing M because the upwash field is further reduced by the model being located offcenter with respect to the Mach cone axis. Therefore, the vortex lift realizable actually decreases with α. But in order to estimate the $K_{v,le}$ variation with α, better supersonic potential-flow solutions are needed.

---

[1]These solutions were obtained by James M. Luckring of Langley Research Center with a recently developed asymmetric version of the computer program described in reference 18.

Rectangular Wing

Figure 15 presents evidence that side-edge vortex lift is present for rectangular wings at supersonic speeds. (The experimental data shown were taken from ref. 21.) At the left of the figure is the change in upper surface pressure with α for two locations, one outside and one inside the tip Mach cone. The values of $\Delta C_{p,u}$ outside the tip cone are well estimated by the potential theory of reference 22, whereas those inside and near the tip trailing edge are underestimated over a wide range of α. At subsonic speeds, this type of nonlinear $\Delta C_{p,u}$ growth with α for a sharp-edge wing would be attributed to vortex flow being present.

The middle graph shows a comparison similar to the left graph except that the difference in c_n at the outboard station is not as extreme as for $\Delta C_{p,u}$. This more linear behavior is attributed to (1) values of $\Delta C_{p,u}$ measured ahead of the illustrated location demonstrating a smaller amount of nonlinear variation with α and (2) the modifying effect of the lower surface pressure in the computation of c_n. The difference in c_n between the potential theory estimate and the data is, therefore, attributed to vortex lift which comes from the side edges located within the tip cones.

Hence, calculation of the attacked-flow side force and use of the suction analogy provide a means of estimating this vortex-lift effect. The linearized supersonic potential-flow solutions of reference 23 have been employed to develop the supersonic $K_{v,se}$ solutions presented in reference 14. These solutions are used herein. The graph at the right shows that: (1) vortex normal force is present in the data; and (2) the data are well estimated by the combination of potential and vortex normal force.

Variation of $K_{v,se}$

Figure 16 shows for two planforms the variation of $K_{v,se}$ with M obtained by using the method of reference 5 at $M \leq 1$ and the results of reference 14 at $M > 1$. Also, selected side-edge suction distributions for each planform are shown. The $K_{v,se}$ values increase with M in the subsonic regime and decrease in the supersonic. The beginning of the supersonic results are set by the Mach number for which the tip cones just intersect along the trailing edge. The short dashed lines used to connect the subsonic and supersonic results are assumed variations. The reasons for the behavior of $K_{v,se}$ with M are contained in the side-edge suction distributions and are now discussed.

For the rectangular wing, increasing the subsonic M is equivalent to decreasing A which in reference 5 was shown to lead to a rectangularization of the distribution and an increase in $K_{v,se}$. However, at supersonic M the side-edge suction distribution again goes to zero at the tip leading edge but now varies linearly over the side edge because of the conical flow nature of the solution. The falloff of $K_{v,se}$ with increasing

supersonic M is the result of two conflicting effects. The first is the reduction in size of the tip Mach cone and the magnitude of the upwash within it, and the second is the increase in sidewash due to the limits of the Mach forecone which eliminate the reducing effects of the other wing panel. The tip cone reduction appears to be the stronger effect.

For the cropped-delta wing, reference 14 illustrates the $K_{v,se}$ reduction which occurs with increasing subsonic M. In figure 16 the distributions are seen to peak at higher values with increasing M. At supersonic M and with a subsonic leading edge, there is an increase in the initial sidewash over the side edge due to the restrictive limits of the Mach forecone at the leading edge of the tip. This is due to the conical-flow assumption which results in the distribution being linear aft of this point. With increasing supersonic M the size of the tip Mach cone and the magnitude of the upwash within it also decrease, leading to a reduction in $K_{v,se}$.

Application

Figure 17 presents a comparison of the aerodynamic characteristics obtained on a cropped-delta wing-body model tested at M = 1.2 (ref. 24) with the results of the present method for the wing alone at the same Mach number. The comparison shows that inclusion of the leading-edge-, side-edge-, and augmented-vortex-lift effects leads to improved agreement. The pitching-moment contributions are obtained by having the vortex lifts act at their respective centroids, and by performing the analytic surface integration, both inside and outside of the tip cone, of the product of the potential-flow lifting pressure (given in ref. 23) and its chordwise position. (See ref. 25.) The potential theory drag curve contains $C_{D,o}$ and is presented for full leading-edge suction and with no separation around the side edges. The other theoretical drag curve also includes $C_{D,o}$.

MULTIPLE LIFTING SURFACES

Vortex-lift estimates have been made up to now for isolated wings, but in this section, multiple lifting surfaces are treated. Examples of these surfaces are wing-tail or wing-canard configurations; however, configurations such as a wing-body can also be considered multiple lifting surfaces when the body is taken to be a lifting one and is represented by a flat surface.

Figure 18 presents applications of the suction analogy to configurations. On the left are the lift results for a slender wing-body, and the data (taken from ref. 26) are well estimated by the combination of potential and vortex lifts. On the right of the figure are the wing lift results for a nonslender configuration. At the top the wing is in the presence of a forebody and at the bottom it is in the presence of a high canard ($z/c_{ref} = 0.185$). The top part shows a C_L variation typical of wings with moderate sweep because they

are known to have low angles of attack for departure and vortex breakdown (ref. 2). However, in the presence of the high canard, a favorable interference results, and even with the reduction in $C_{L,p}$ on the wing, due to canard downwash, the predicted amount of vortex lift is developed on the wing. The data (taken from ref. 27) are well predicted over the range of α and reach higher C_L values than those for the wing in the presence of the forebody.

Figure 19 presents the effect on the wing lift characteristics of changing the canard position. From the figure it can be seen that both the high canard with anhedral ($\phi = -18.6^o$) and the coplanar canard have a favorable interference effect on the wing. In neither case has the augmented vortex lift due to the leading-edge vortex of the canard been taken into account. This omission is proper for the canard in the anhedral position but questionable in the coplanar arrangement. This vortex lift was omitted because an appropriate $\tilde{c}$ has yet to be determined.

CONCLUDING REMARKS

This paper has presented some recent extensions of the suction analogy for the estimation of vortex lift from the side edges and from the downstream effects of the leading-edge shed vortex. Applications of these extensions have resulted in an improved estimating capability for a wide range of isolated sharp-edge planforms and also for multiple lifting surfaces. Hence, the suction analogy concept can now have wider applicability at both subsonic and supersonic speeds, especially in the preliminary design cycle.

The following are areas in which additional research is needed:

(1) An improved supersonic potential-flow program that properly accounts for the changing proximity of the model and its Mach cone with angle of attack

(2) Development of a method for predicting the location and strength of the vortex flow originating on rounded-edge wings and the enlargements of the influenced region with angle of attack

(3) Surface pressure distributions for wings which have vortex flows originating along the leading and side edges for use in critical design analyses

REFERENCES

1. Polhamus, Edward C.: A Concept of the Vortex Lift of Sharp-Edge Delta Wings Based on a Leading-Edge-Suction Analogy. NASA TN D-3767, 1966.

2. Wentz, William H., Jr.; and Kohlman, David L.: Wind Tunnel Investigations of Vortex Breakdown on Slender Sharp-Edged Wings. NASA CR-98737, 1968.

3. Polhamus, Edward C.: Charts for Predicting the Subsonic Vortex-Lift Characteristics of Arrow, Delta, and Diamond Wings. NASA TN D-6243, 1971.

4. Polhamus, Edward C.: Predictions of Vortex-Lift Characteristics by a Leading-Edge Suction Analogy. J. Aircraft, vol. 8, no. 4, Apr. 1971, pp. 193-199.

5. Lamar, John E.: Extension of Leading-Edge-Suction Analogy to Wings With Separated Flow Around the Side Edges at Subsonic Speeds. NASA TR R-428, 1974.

6. Lamar, John E.: A Modified Multhopp Approach for Predicting Lifting Pressures and Camber Shape for Composite Planforms in Subsonic Flow. NASA TN D-4427, 1968.

7. Bradley, R. G.; Smith, C. W.; and Bhateley, I. C.: Vortex-Lift Prediction for Complex Wing Planforms. J. Aircraft, vol. 10, no. 6, June 1973, pp. 379-381.

8. Mendenhall, Michael R.; and Nielsen, Jack N.: Effect of Symmetrical Vortex Shedding on the Longitudinal Aerodynamic Characteristics of Wing-Body-Tail Combinations. NASA CR-2473, 1975.

9. Lamar, John E.; and Gloss, Blair B.: Subsonic Aerodynamic Characteristics on Interacting Lifting Surfaces With Separated Flow Around Sharp Edges Predicted by Vortex-Lattice Method. NASA TN D-7921, 1975.

10. Gersten, K.: Calculation of Non-Linear Aerodynamic Stability Derivative of Aeroplanes. AGARD Rep. 342, Apr. 1961.

11. Garner, H. C.; and Lehrian, Doris E.: Non-Linear Theory of Steady Forces on Wings With Leading-Edge Flow Separation. NPL Aero Rep. 1059, Brit. A.R.C., Feb. 15, 1963.

12. Belotserkovskii, S. M. (J. W. Palmer, transl.): Calculation of the Flow About Wings of Arbitrary Planform at a Wide Range of Angle of Attack. Libr. Transl. No. 1433, Brit. R.A.E., Feb. 1970.

13. Flax, A. H.; and Lawrence, H. R.: The Aerodynamics of Low-Aspect-Ratio Wings and Wing-Body Combination. Third Anglo-American Aeronautical Conference, Jean Bradbrooke and E. C. Pike, eds., Royal Aeronautical Soc., 1952, pp. 363-398.

14. Lamar, John E.: Prediction of Vortex Flow Characteristics of Wings at Subsonic and Supersonic Speeds. AIAA Paper No. 75-249, Jan. 1975.

15. Snyder, Melvin H., Jr.; and Lamar, John E.: Application of the Leading-Edge-Suction Analogy to Prediction of Longitudinal Load Distribution and Pitching Moments for Sharp-Edged Delta Wings. NASA TN D-6994, 1972.

16. Hancock, G. J.: Some Aspects of Subsonic Linearised Wing Theory, With Reference to Second Order Forces and Moments. Brit. A.R.C.34 689, Mar. 1973.

17. Davenport, Edwin E.; and Huffman, Jarrett K.: Experimental and Analytical Investigation of Subsonic Longitudinal and Lateral Aerodynamic Characteristics of Slender Sharp-Edge 74° Swept Wings. NASA TN D-6344, 1971.

18. Margason, Richard J.; and Lamar, John E.: Vortex-Lattice FORTRAN Program for Estimating Subsonic Aerodynamic Characteristics of Complex Planforms. NASA TN D-6142, 1971.

19. Fox, Charles H., Jr.; and Lamar, John E.: Theoretical and Experimental Longitudinal Aerodynamic Characteristics of an Aspect Ratio 0.25 Sharp-Edge Delta Wing at Subsonic, Supersonic, and Hypersonic Speeds. NASA TN D-7651, 1974.

20. Davenport, Edwin E.: Aerodynamic Characteristics of Three Slender Sharp-Edge 74° Swept Wings at Subsonic, Transonic, and Supersonic Mach Numbers. NASA TN D-7631, 1974.

21. Kaattari, George E.: Pressure Distributions on Triangular and Rectangular Wings to High Angles of Attack – Mach Numbers 1.45 and 1.97. NACA RM A54D19, 1954.

22. Woodward, Frank A.: Analysis and Design of Wing-Body Combinations at Subsonic and Supersonic Speeds. J. Aircraft, vol. 5, no. 6, Nov.-Dec. 1968, pp. 528-534.

23. Malvestuto, Frank S., Jr.; Margolis, Kenneth; and Ribner, Herbert S.: Theoretical Lift and Damping in Roll at Supersonic Speeds of Thin Sweptback Tapered Wings With Streamwise Tips, Subsonic Leading Edges, and Supersonic Trailing Edges. NACA Rep. 970, 1950. (Supersedes NACA TN 1860.)

24. Hightower, Ronald C.: Lift, Drag, and Pitching Moment of Low-Aspect-Ratio Wings at Subsonic and Supersonic Speeds – Comparison of Three Wings of Aspect Ratio 2 of Rectangular, Swept-Back, and Triangular Plan Form, Including Effects of Thickness Distribution. NACA RM A52L02, 1953.

25. Malvestuto, Frank S., Jr.; and Hoover, Dorothy M.: Lift and Pitching Derivatives of Thin Sweptback Tapered Wings With Streamwise Tips and Subsonic Leading Edges at Supersonic Speeds. NACA TN 2294, 1951.

26. Henderson, William P.: Studies of Various Factors Affecting Drag Due to Lift at Subsonic Speeds. NASA TN D-3584, 1966.

27. Gloss, Blair B.: The Effect of Canard Leading-Edge Sweep and Dihedral Angle on the Longitudinal and Lateral Aerodynamic Characteristics of a Close-Coupled Canard-Wing Configuration. NASA TN D-7814, 1974.

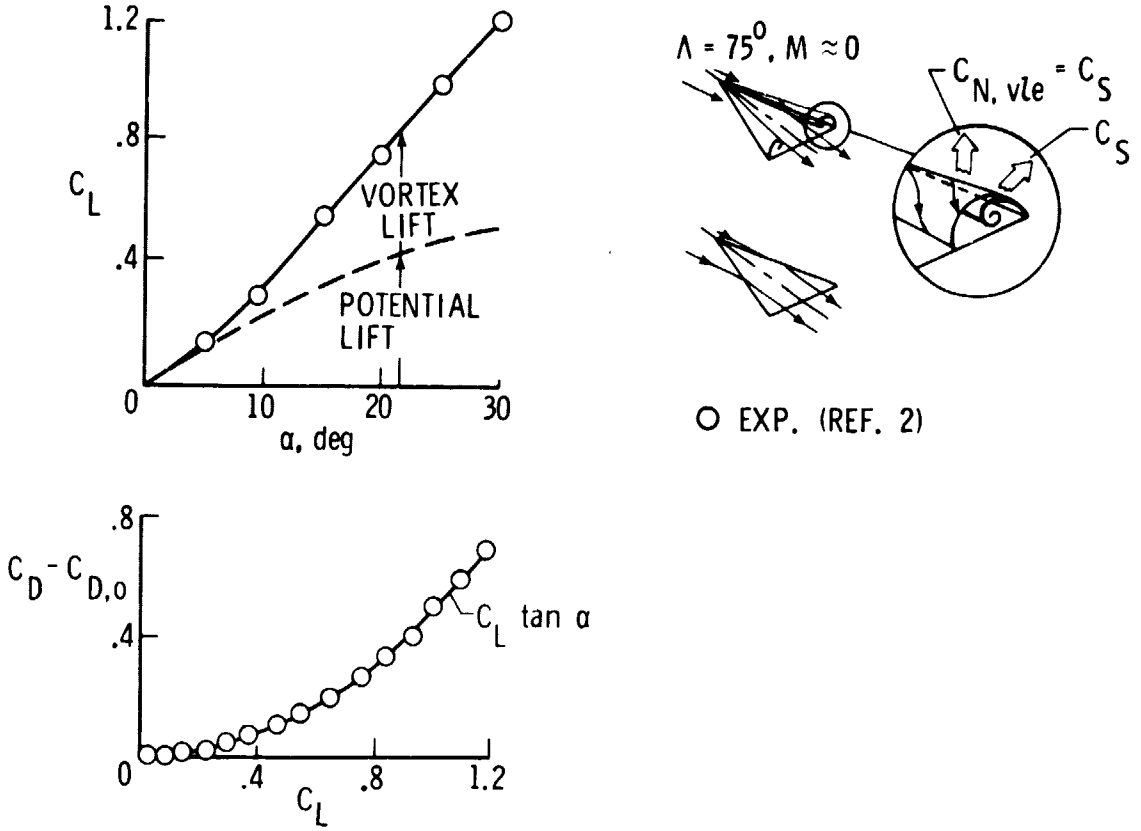

Figure 1.- Original application of suction analogy.

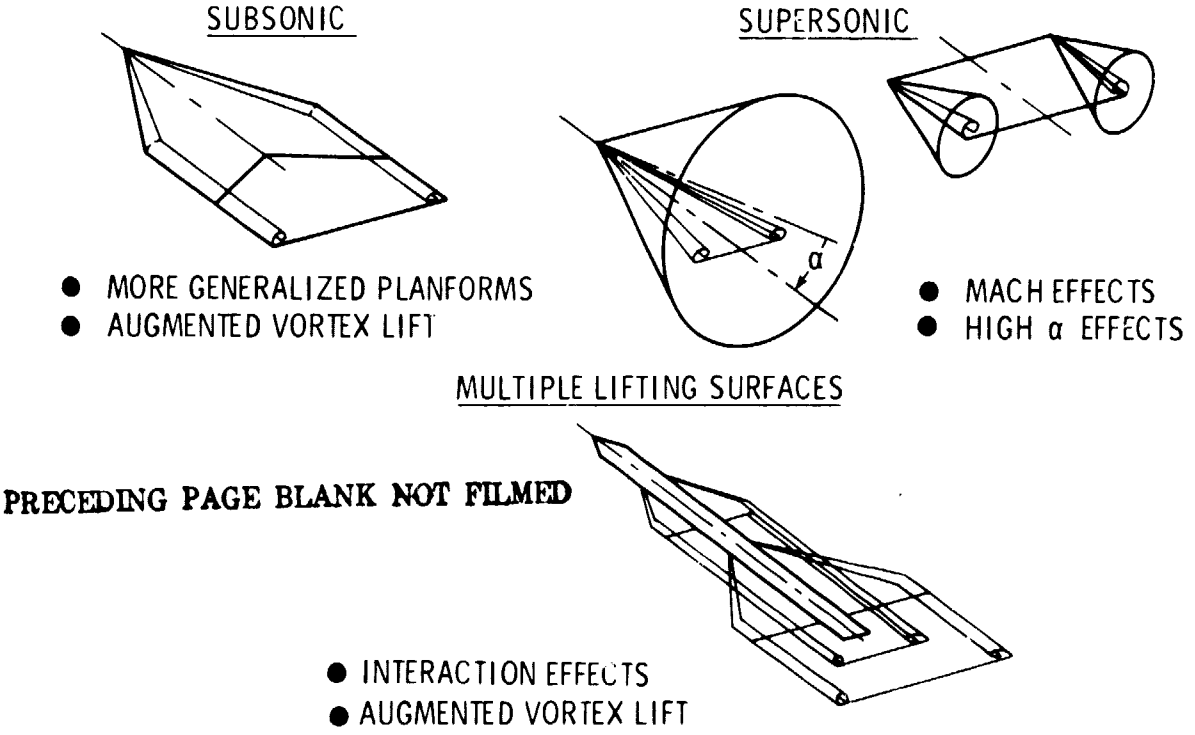

PRECEDING PAGE BLANK NOT FILMED

Figure 2.- Some recent applications of suction analogy to vortex-lift estimates.

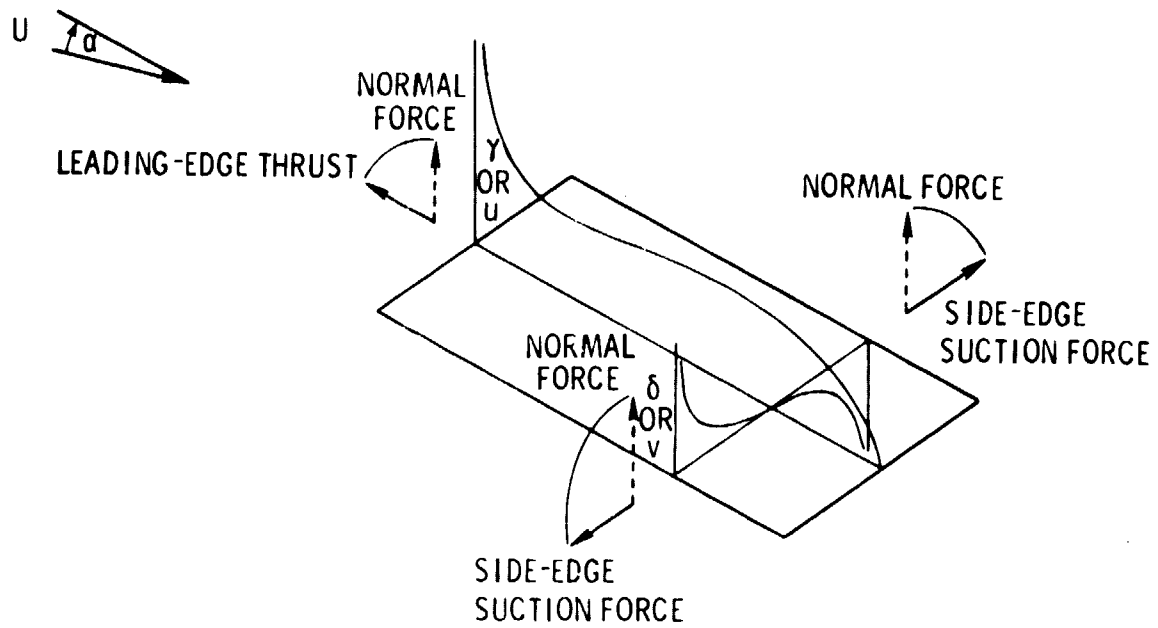

Figure 3.- Vortex-lift concept: Suction analogy applied to leading edge and side edge.

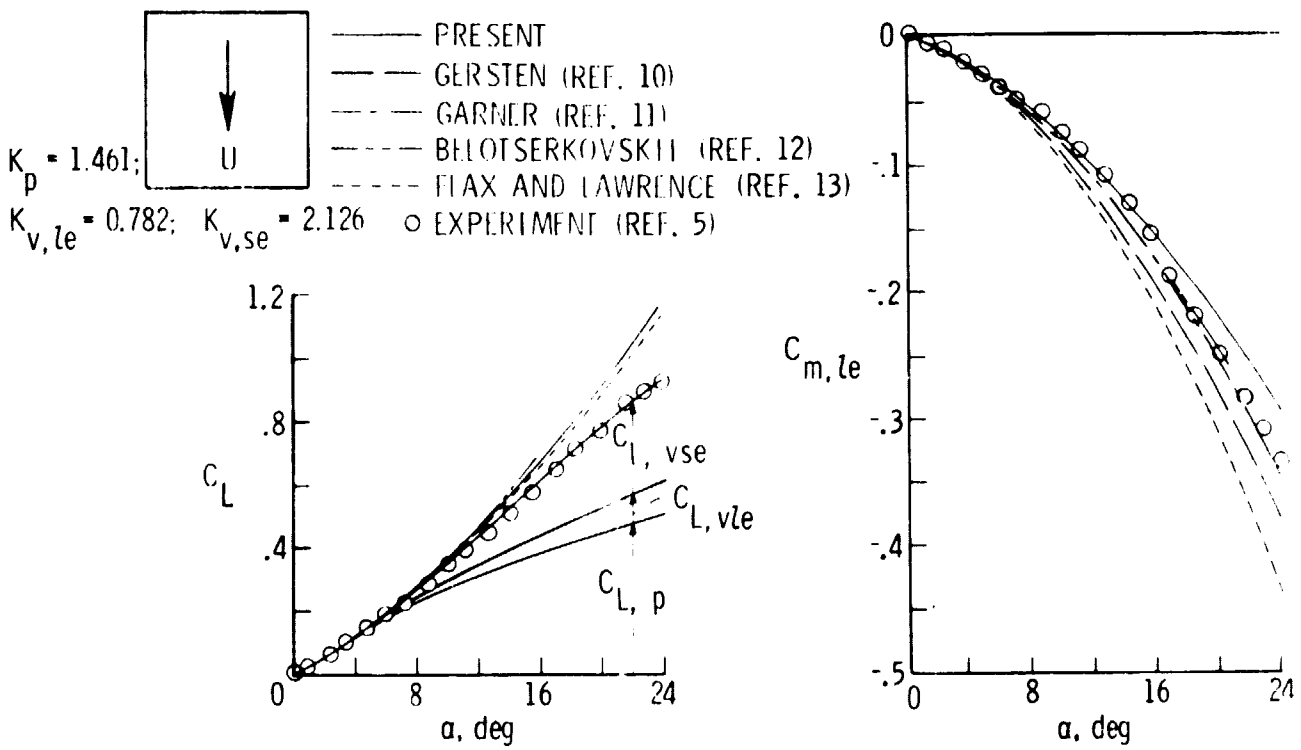

Figure 4.- Aerodynamic characteristics of rectangular wing. A = 1; M ≈ 0.

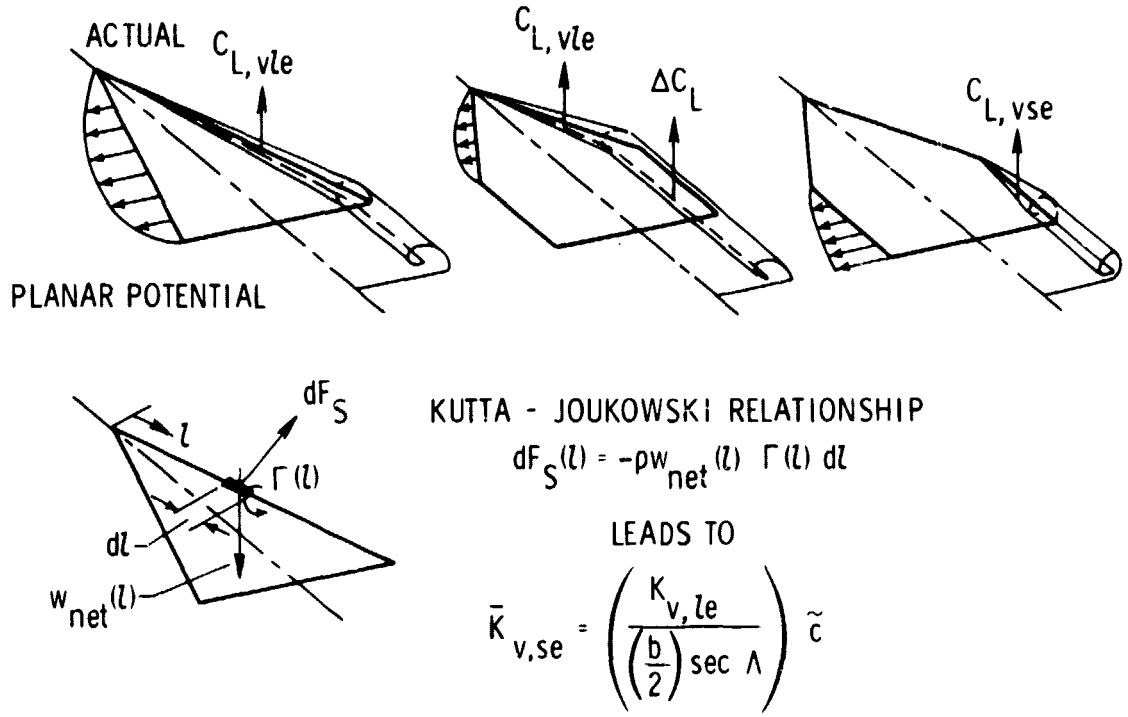

Figure 5.- Concept of augmented vortex lift.

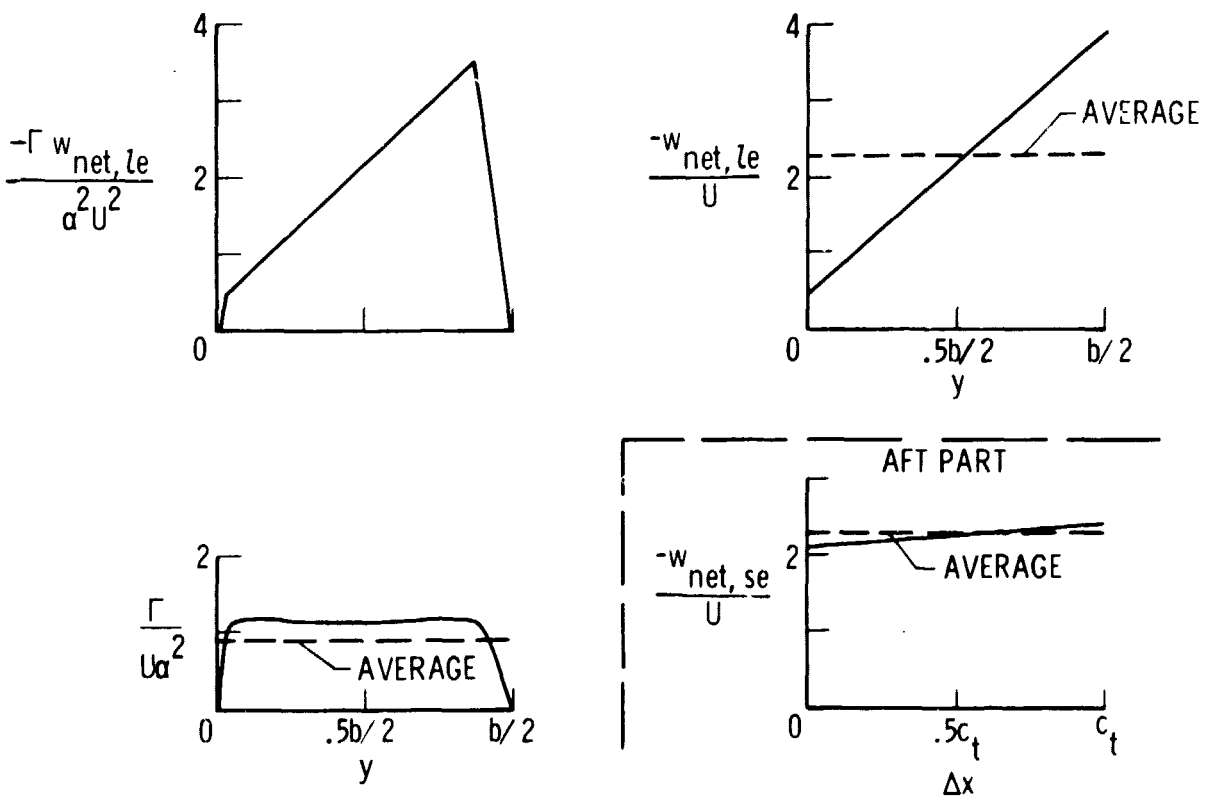

Figure 6.- Variables used in augmented-vortex-lift determination. Cropped-delta wings: delta part idealized.

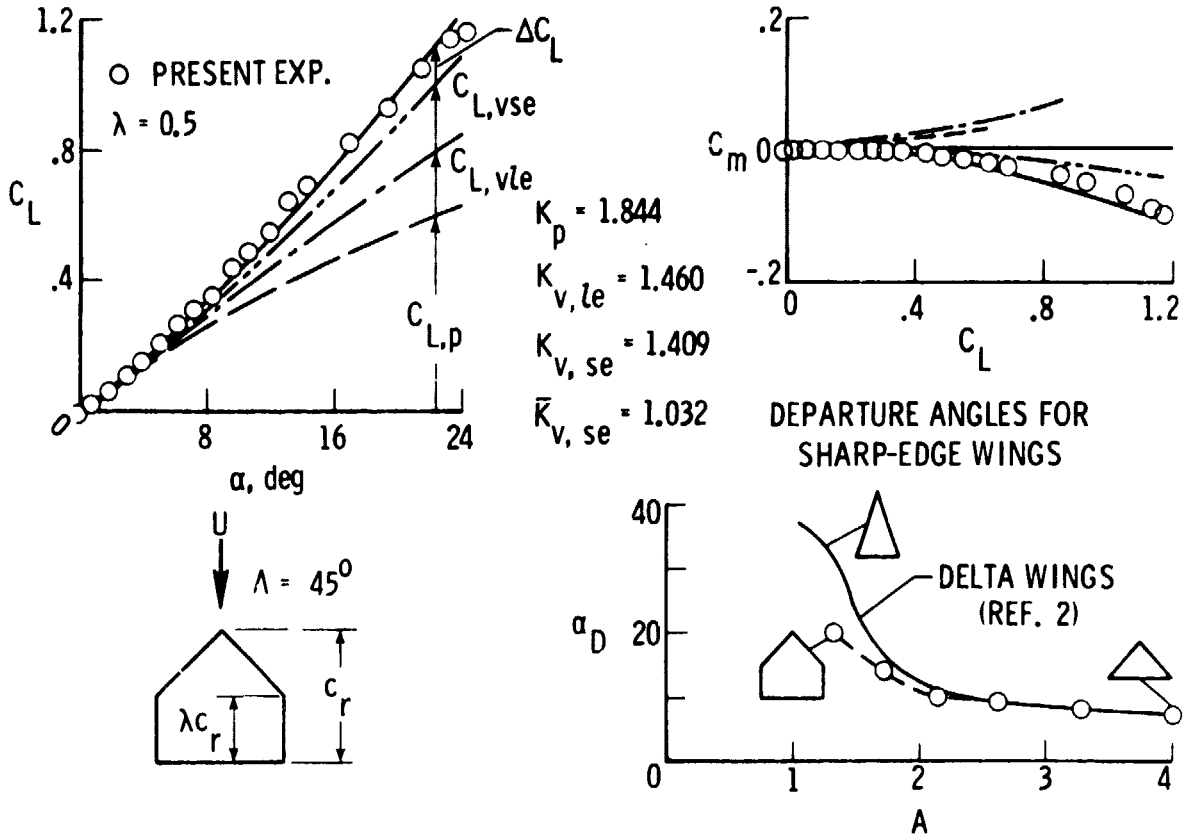

Figure 7.- Aerodynamic characteristics of cropped-delta wings. M ≈ 0.

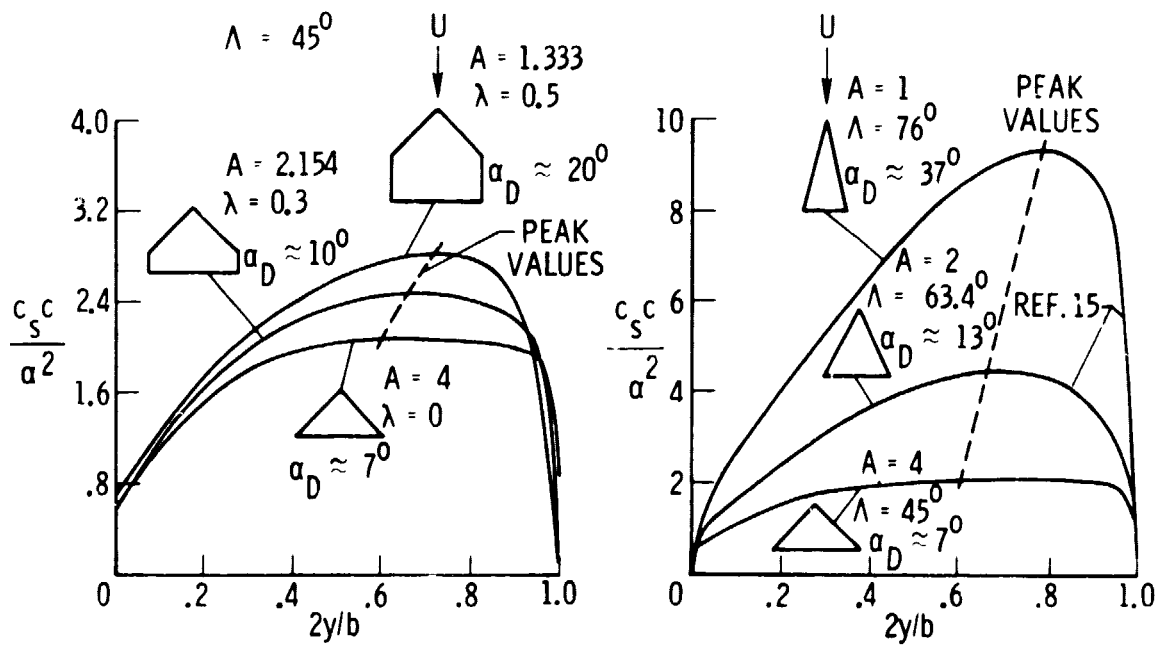

Figure 8.- Leading-edge suction distributions and departure angle of attack. M ≈ 0.

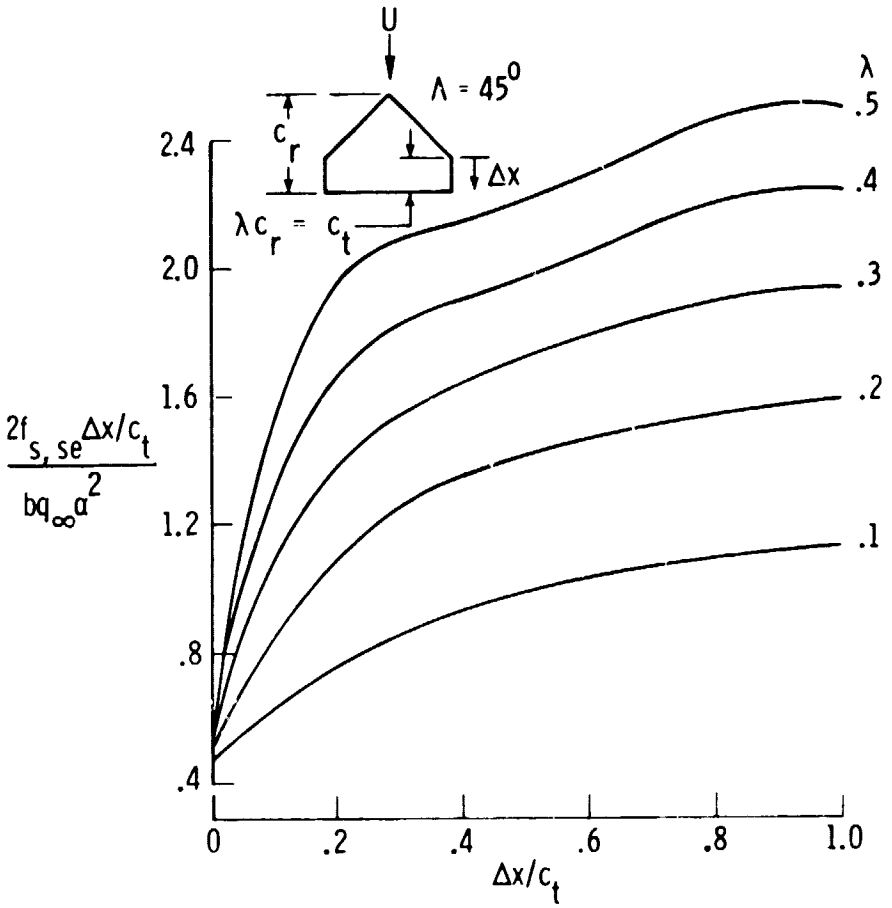

Figure 9.- Side-edge suction distribution for cropped-delta wings. $M \approx 0$.

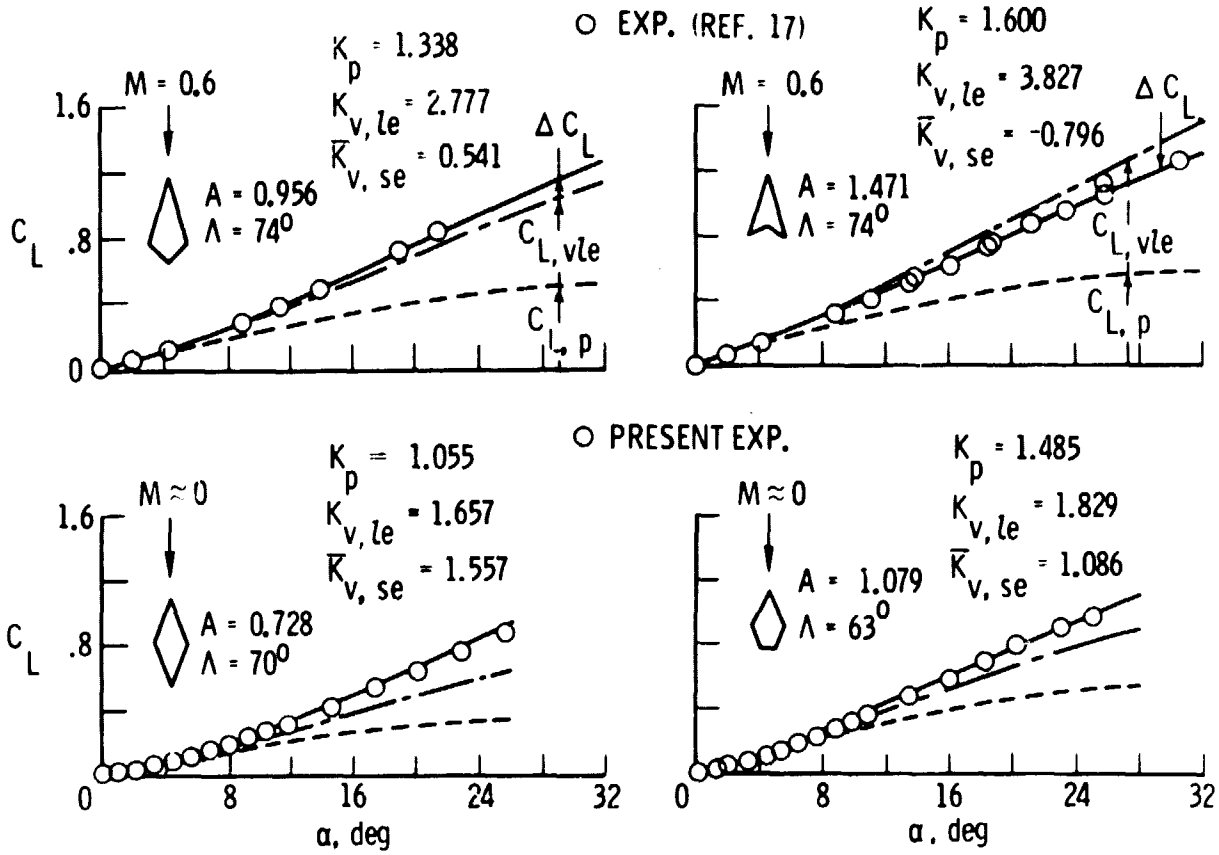

Figure 10.- Lift characteristics of pointed wings.

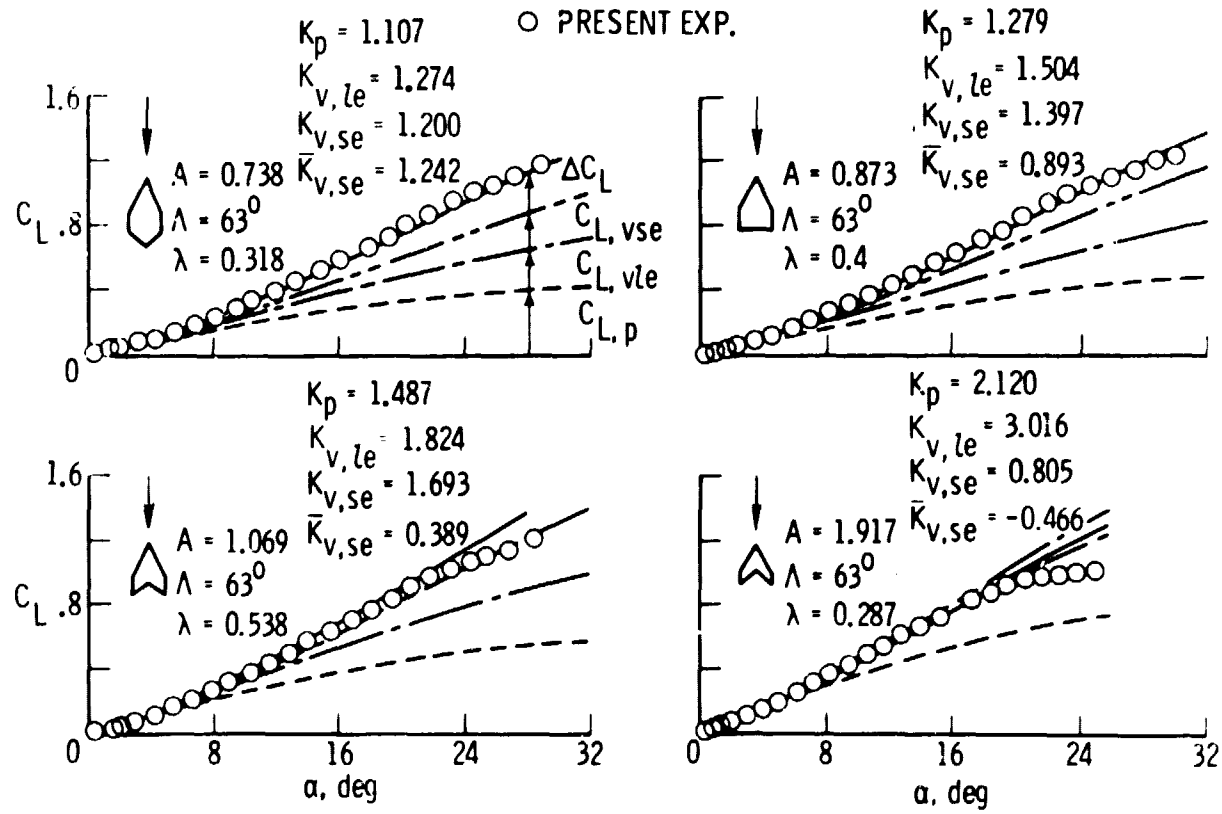

Figure 11.- Lift characteristics of wings with streamwise tips. M ≈ 0.

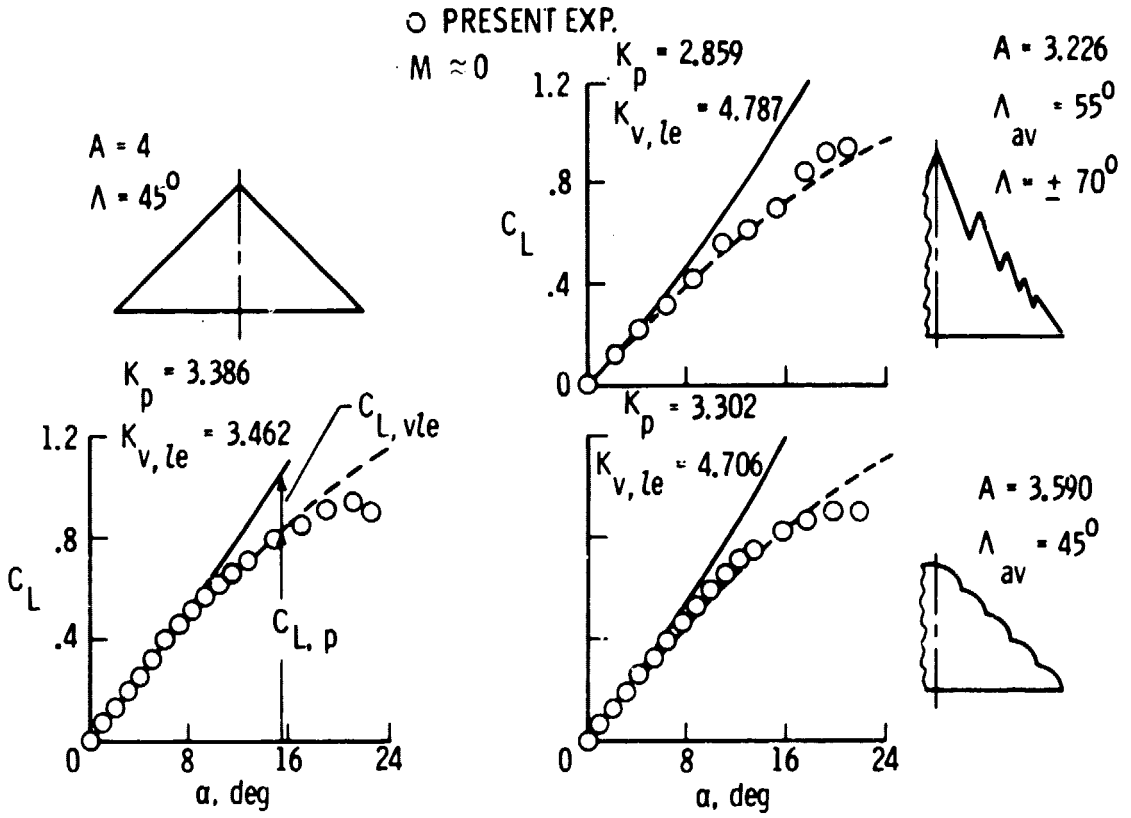

Figure 12.- Attempts to improve vortex lift on pointed wings of moderate sweep.

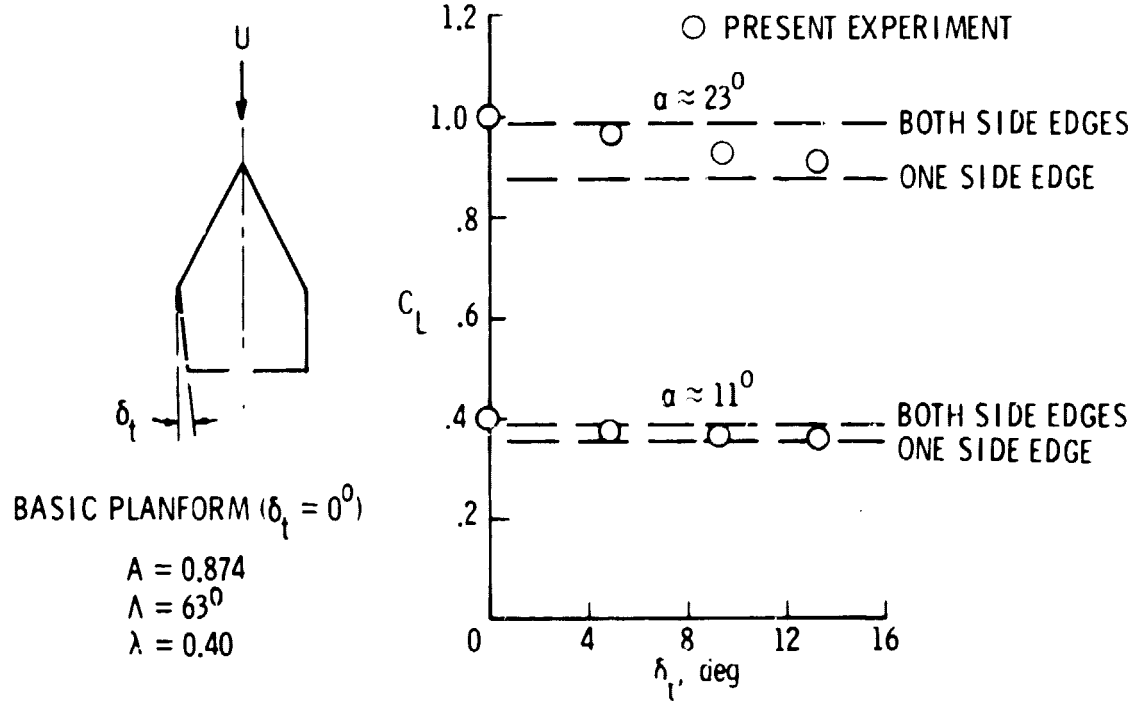

Figure 13.- Estimates of C_L for asymmetrical wings. $M \approx 0$.

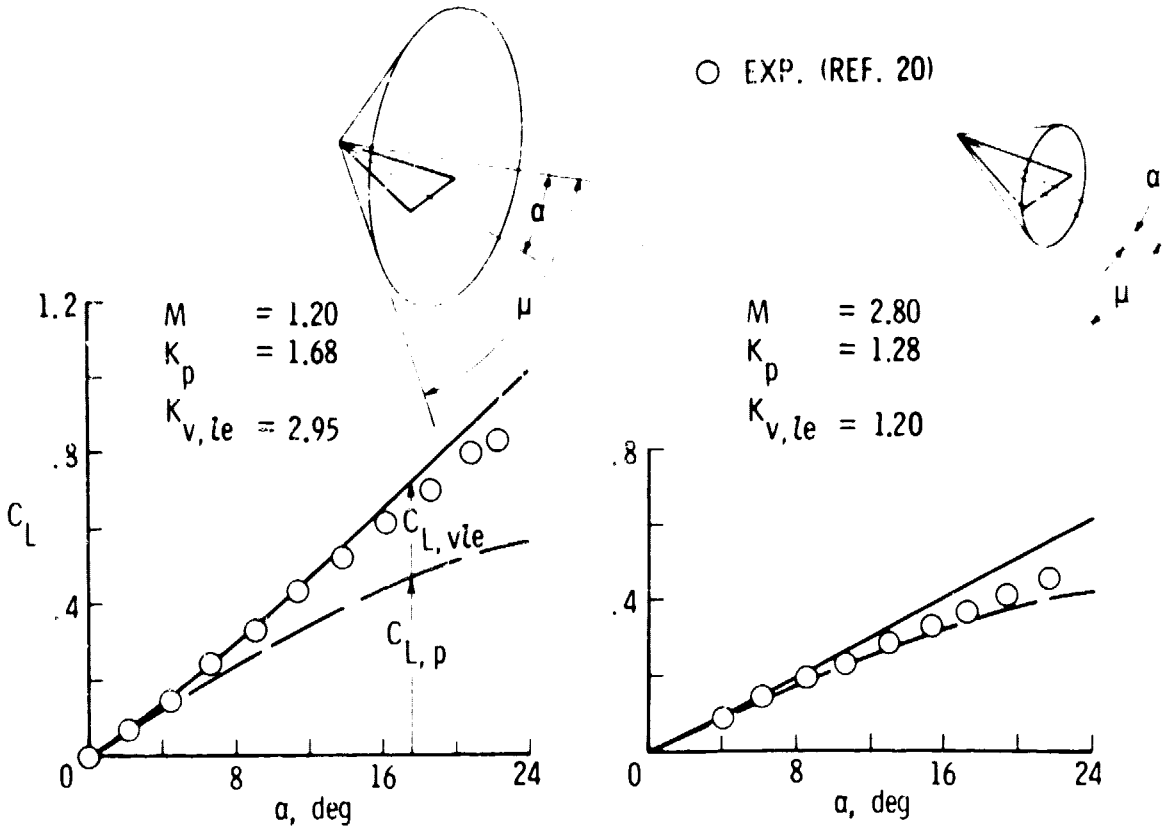

Figure 14.- Effect of supersonic Mach number on C_L for delta wing. A = 1.1.

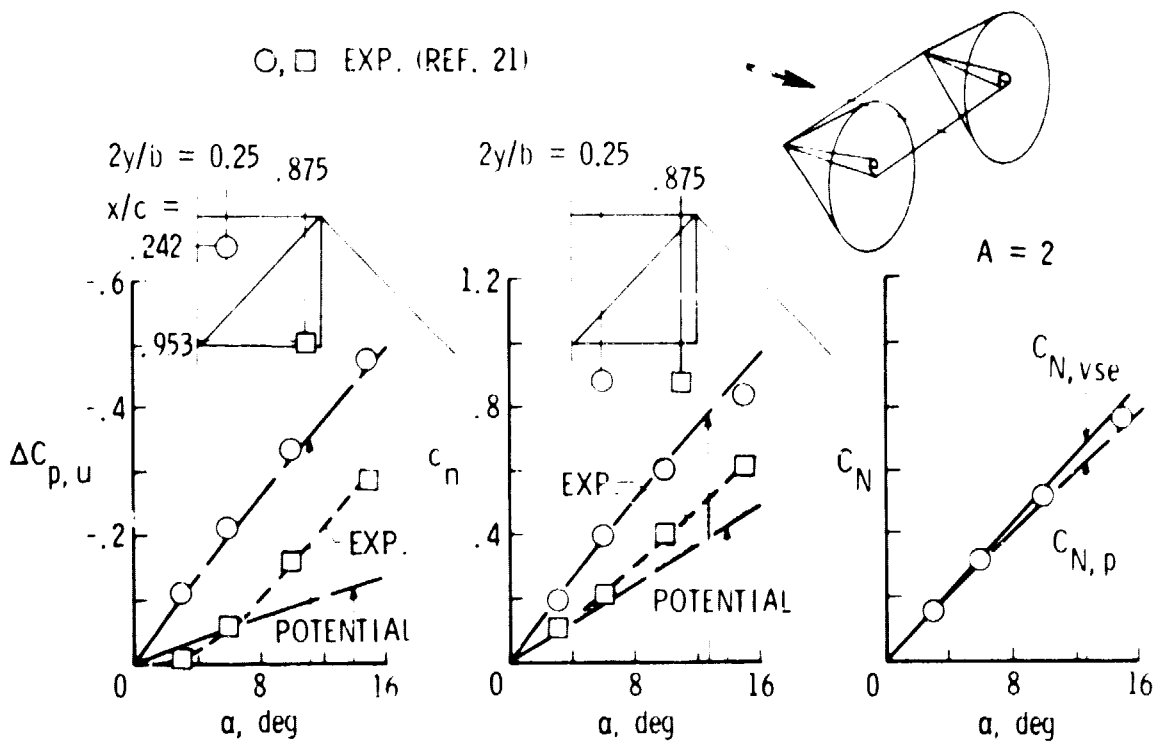

Figure 15.- Evidence of vortex lift within tip Mach cone. M = 1.45.

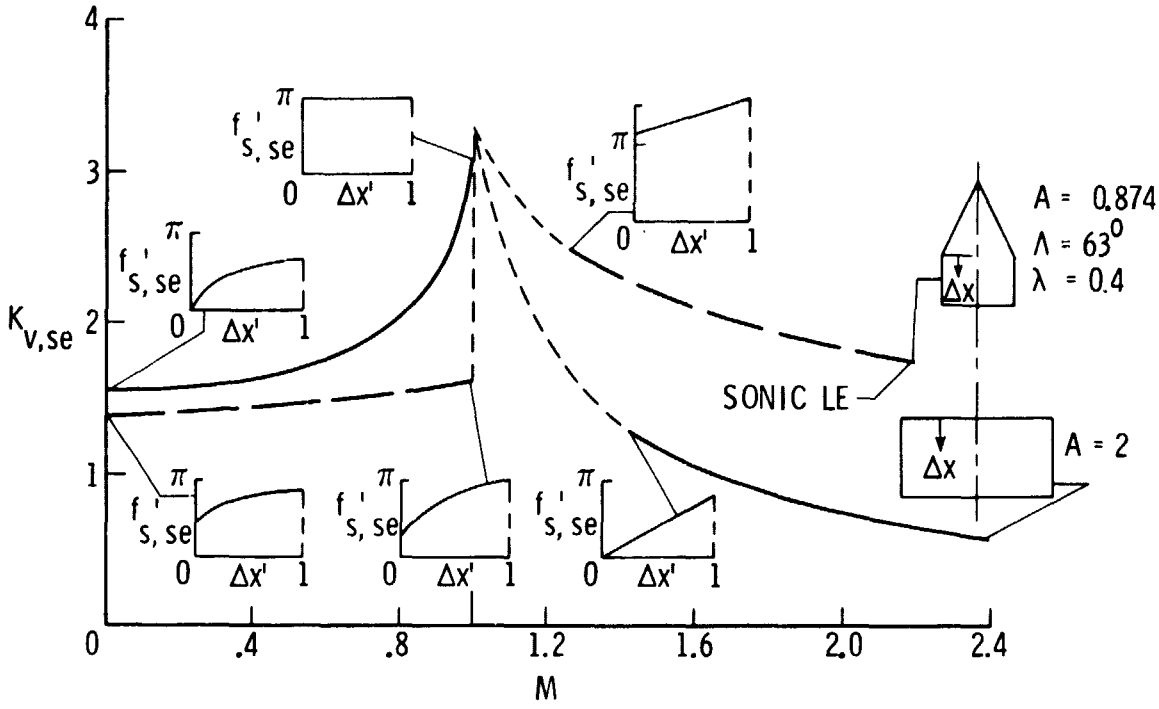

Figure 16.- Variation of $K_{v,se}$ with Mach number for two wings including selected side-edge suction distributions.

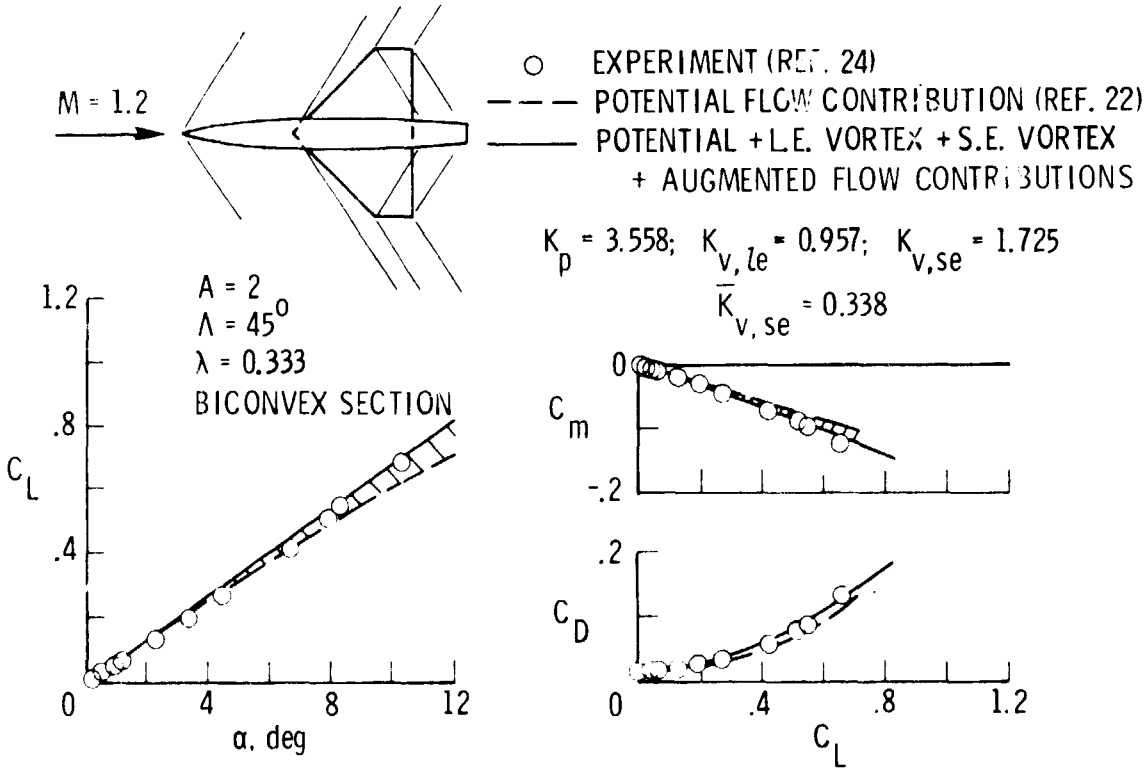

Figure 17.- Aerodynamic characteristics of a cropped-delta wing-body.

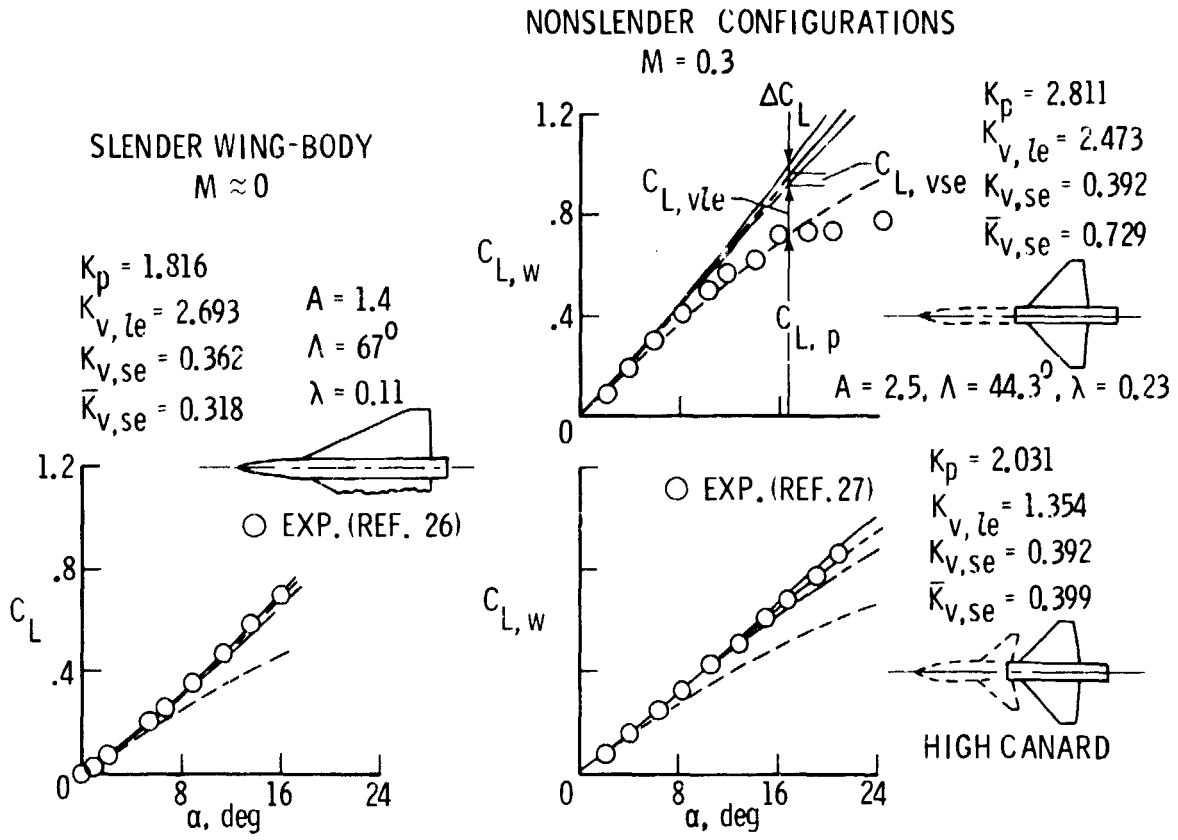

Figure 18.- Suction analogy applications to configurations.

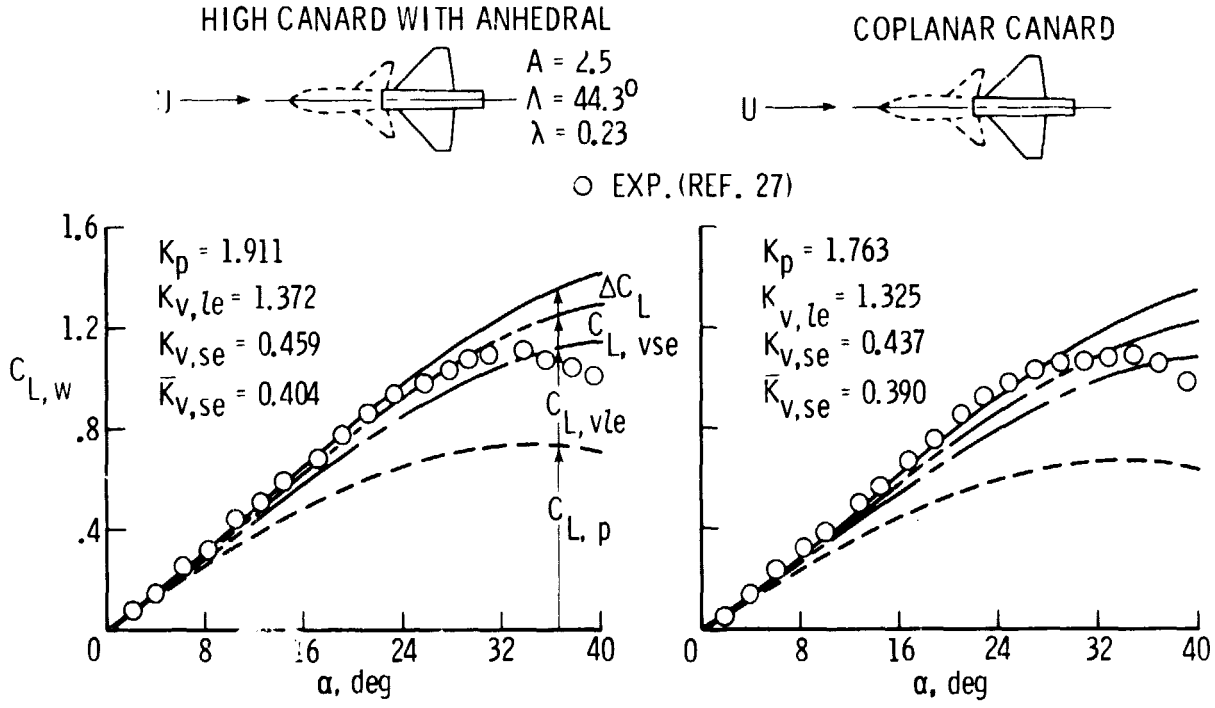

Figure 19.- Effect of canard position on wing lift characteristics for wing-canard configuration. M = 0.3.